ELSEVIER

0966-9795(95)00013-5

Intermetallics 4 (1996) 23–29
©1995 Elsevier Science Limited
Printed in Great Britain. All rights reserved
0966-9795/96/$09.50

Phase transformations in an *in situ* Nb-reinforced Nb_3Al intermetallic composite

C. D. Bencher, L. Murugesh, K. T. V. Rao & R. O. Ritchie

Department of Materials Science and Mineral Engineering, University of California at Berkeley, Berkeley, California 94720–1760, USA

(Received 20 June 1994; accepted 26 January 1995)

The development of two-phase Nb/Nb_3Al *in situ* composite microstructures by thermal treatment in a Nb–6wt.%Al alloy, processed through powder-metallurgy techniques, is examined in detail using transmission and scanning electron microscopy. Observations reveal that the precipitation of Nb_3Al in a heavily dislocated Nb solid solution matrix initiates at grain boundaries and progresses along the <110> and <211> directions in the matrix and Nb_3Al precipitate, respectively; the precipitates eventually fuse into small, elongated grains with 1–10 μm dimensions. The evolution of the *in situ* composite microstructure from the hot-pressed equiaxed structure proceeds by a diffusion-controlled nucleation and growth transformation and not by a massive transformation. The lamellar microstructure of the alloy displays a five-fold increase in toughness over unreinforced Nb_3Al primarily due to crack bridging and plastic deformation associated with the ductile Nb phase.

Key words: Nb_3Al, *in situ* composites, fracture toughness.

1 INTRODUCTION

Niobium–aluminide intermetallic alloys are currently being investigated as potential ultra-high temperature structural materials for high-performance gas turbine engine applications.[1] Among the various intermetallic compounds in the Nb–Al system,[2] namely Nb_3Al, Nb_2Al and $NbAl_3$ (Fig. 1), Nb_3Al is the most promising because of its higher melting temperature, oxidation resistance and creep properties.[3,4] However, like many intermetallics that exhibit high melting points and high elastic moduli, Nb_3Al has relatively low symmetry due to its A-15 crystal structure. While the A-15 structure is responsible for the high temperature strength of Nb_3Al, it concurrently results in limited ductility and poor fracture toughness at ambient temperatures.[5,6]

Addition of ductile phases in the microstructure has been shown to be an effective means for improving the toughness of brittle materials primarily through crack bridging by intact ductile ligaments in the crack wake.[7–15] Many ceramics and intermetallics, including Nb_3Al, have successfully employed this approach to enhance their fracture properties at room temperature. Such ductile-particle reinforced Nb/Nb_3Al composite microstructures can be fabricated by powder-metallurgy (P/M) techniques by blending and hot pressing the individual phases with possible additional thermal treatment to enable *in situ* precipitation of the Nb + Nb_3Al through a peritectic reaction.[13,14] In addition, magnetron-sputtering[15] and conventional casting and thermomechanical processing[3,4] have also been used to develop two-phase Nb/Nb_3Al microstructures. Of the various processing methods, the P/M route with thermal treatment to enable *in situ* phase formation has the advantage that solid-state reactions, at temperatures significantly below the solidus, can be utilized in fabricating near-net shaped products. Since such techniques require an understanding of phase transformations in the alloy system, the intent of this paper is to examine the microscopic aspects of Nb + Nb_3Al precipitation in a powder-processed Nb–18 at.% (6 wt.%) Al alloy.

This work was supported by the United States Air Force Office of Scientific Research under Grant No. F49620-93-1-0107.

2 MATERIALS AND EXPERIMENTAL PROCEDURES

The Nb/Nb_3Al composite was processed by hot pressing *in vacuo* (at 1650°C, 37 MPa pressure for 10 min) reactively-synthesized (at 1450°C for 1 h), pure Nb (-325 mesh, 99.8% pure) and Al (-325

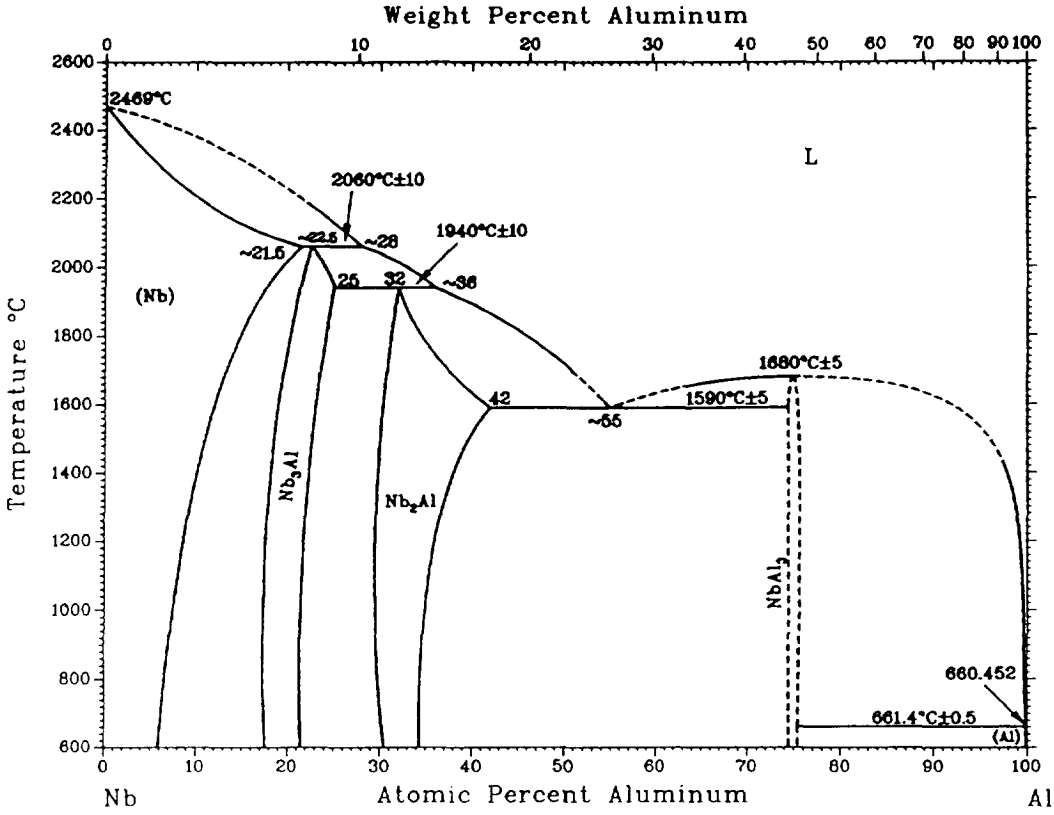

Fig. 1. The Nb–Al phase diagram showing the various niobium aluminide intermetallic compounds, Nb_3Al (A-15), Nb_2Al and $NbAl_3$.[2]

mesh, 99.33% pure) powders mixed in the ratio of Nb–18 at.% Al (6 wt.% Al). Hot-pressed samples were thermally treated in an inert argon atmosphere at 1800°C for 1, 4 and 24 h, furnace cooled (15°C/min) to room temperature, and subsequently annealed at 1450°C for 24 h to reduce internal stresses and consolidate the microstructure; complete processing details are given in Ref. 13.

Sections of the specimens were metallographically polished, dimpled and ion milled using a cold stage (3 kV, angle of incidence ~11°) following standard transmission electron microscopy (TEM) sample preparation techniques. The inherently different rates of removal for Nb and Nb_3Al during ion milling often led to thickness variations in TEM foils; as a result, thickness extinction contours were common along Nb/Nb_3Al interfaces. Imaging was performed using Philips EM301 and EM 400 TEMs operating at 100 kV. Polished and etched samples were also examined using an ISI-DS 130C scanning electron microscope (SEM) equipped with an energy dispersive X-ray spectrometer. Fracture toughness was measured using 25 mm wide and 2·5 mm thick disk-shaped compact tension DC(T) samples following ASTM Standard E-399;[16] specimens were fatigue precracked and monotonically loaded to failure. Vickers diamond indents were used to estimate yield strength of the alloy; flexure properties were evaluated using 4 mm square and 12 mm long beams loaded in four-point bending.

3 RESULTS AND DISCUSSION

3.1 Microstructure

The evolution of two-phase Nb/Nb_3Al microstructures is detailed in Fig 2. Hot pressing of the synthesized Nb–Al powder yields a composite microstructure consisting of ~2–5 μm-sized, equiaxed Nb particles in an Nb_3Al matrix (Fig. 2(a)). Thermal treatment at 1800°C initially transforms the entire microstructure into a uniform Nb–Al solid solution (Nb_{ss}) matrix. After ~1 h, the decomposition of Nb_{ss} into the dual-phase lamellar structure initiates with the heterogenous nucleation of small rod-like ordered Nb_3Al precipitates along Nb_{ss} grain boundaries, as shown in Fig. 2(b). The precipitates grow (presumably by removing Al atoms from the bcc Nb_{ss} phase on either side) into a deformed and supersaturated Nb_{ss}, and fuse together forming an elongated lamellar structure. Due to the depletion of Al surrounding the Nb_3Al phase. the subsequent Nb_3Al precipitate nucleates

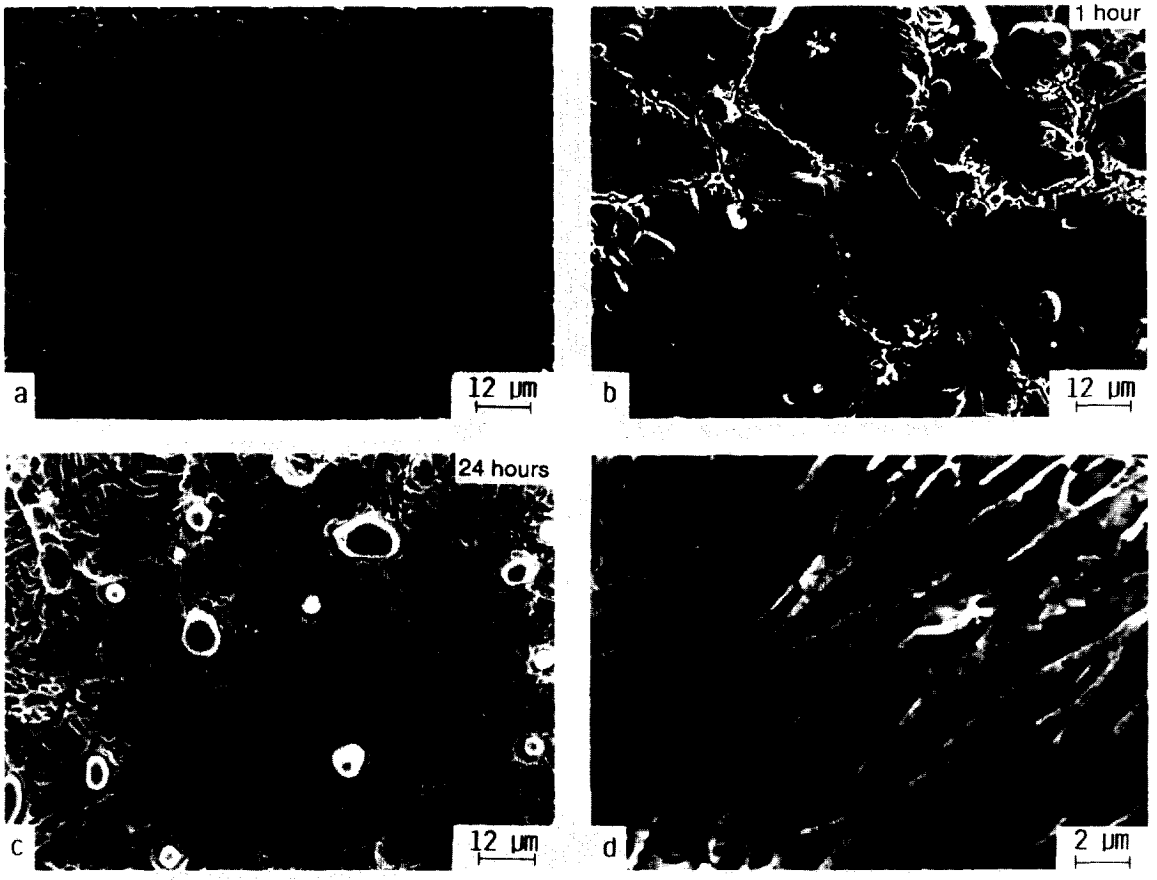

Fig. 2. Scanning electron micrographs depicting the microstructural development in the Nb–18 at.% Al alloy following (a) hot pressing at 1650°C, (b) hot pressing at 1650°C + 1 h at 1800°C, and (c, d) hot pressing at 1650°C + 24 h at 1800°C at various magnifications. Note the heterogeneous nucleation of Nb_3Al along Nb_{ss} grain boundaries.

on the top of, or in parallel to, the existing one, accounting for the lamellar growth of the Nb_3Al colonies. The transformation is rather slow requiring 24 h at 1800°C for completion, following which the structure evolves into a fully-lamellar microstructure with a filamentary Nb morphology, ~0·5–2 μm in thickness, (Figs 2(c, d)). TEM observations of the microstructure in Fig. 3 reveal the two-phase composite microstructure consisting of lamellar Nb_3Al precipitates in a heavily dislocated Nb_{ss} matrix.

Approximate phase compositions were determined using energy dispersive X-ray spectroscopy (EDS); these revealed that the Nb_3Al intermetallic phase contains off-stochiometric amounts of aluminum (~13·8 at.% Al). Other studies[17] also report similar differences in stochiometry during growth of the ordered A-15 precipitate from the supersaturated parent matrix. The off-equilibrium composition of Nb_3Al resulted in a slightly supersaturated Nb_{ss} matrix (~10·2 at.% Al), which accounts for the slight (~2%) reduction in interplanar spacings (Table 1) determined from X-ray diffraction measurements[13] and selected-area-diffraction patterns in Fig. 3. The overall microstructure was found to contain ~14·5 at.% Al suggesting that some aluminum has been lost by evaporation during high temperature processing of the Nb–18 at.% Al powders.

3.2 Phase transformation

The transformation between Nb_{ss} and Nb_3Al has been reported to possess characteristics of both nucleation-growth and martensitic mechanisms, and is referred to as a massive transformation.[18] Massive transformations have been observed upon cooling Nb_{ss} into the single-phase Nb_3Al region over the 18–23 at.% Al composition range; niobium solid solutions, both in the high-temperature single-phase (18–22 at.% Al) and two-phase (22–23 at.% Al) regions, form acicular Nb_3Al structures upon cooling. Such massive transformations can occur in alloy systems where the high-temperature and low-temperature phases, at identical composition, are separated by a two-phase region, and providing the diffusional rates are sufficiently slow.[19] In the case of Nb_3Al, slow diffusion of Al

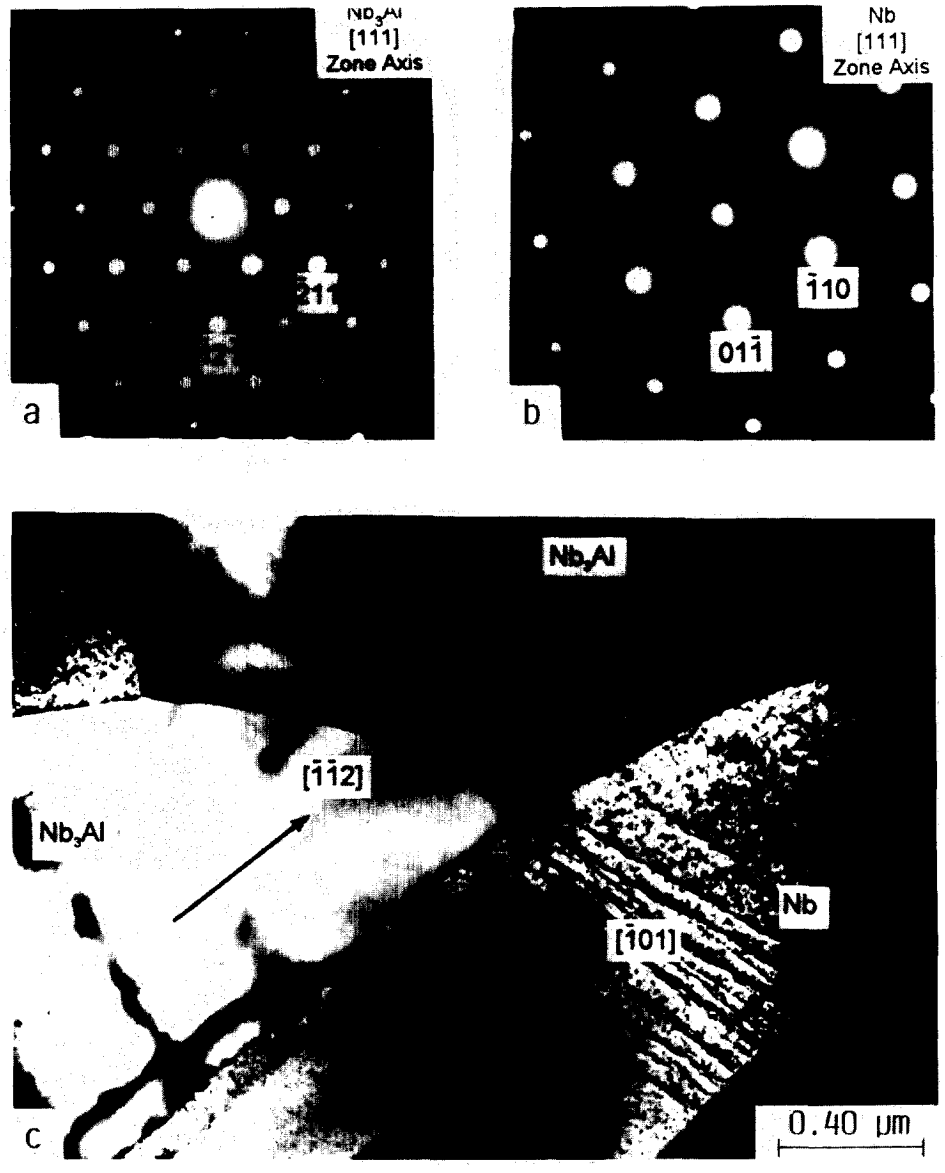

Fig. 3. Selected-area diffraction patterns from the (a) Nb_3Al precipitate, and (b) Nb_{ss} regions in (c) the bright-field TEM micrograph of the Nb/Nb_3Al lamellar composite microstructure. Note the dislocations in the Nb_{ss} solid solution regions and bend extinction contours within the ordered Nb_3Al precipitates.

Table 1. Interplanar spacings for Nb and Nb_3Al structures

Nb (bcc, $a_o = b_o = c_o = 3{\cdot}30$ Å)			Nb_3Al (A-15, $a_o = b_o = c_o = 5{\cdot}19$ Å)		
hkl	literature d_{hkl}(Å)	measured d_{hkl}(Å)	hkl	literature d_{hkl}(Å)	measured d_{hkl}(Å)
110	2·333	2·273	110	3·668	3·643
200	1·650		200	2·594	
211	1·347	1·320	210	2·320	
220	1·167		211	2·118	2·110
310	1·044		220	1·834	
222	0·953		310	1·640	
321	0·882	0.867	222	1·497	
400	0·825		320	1·439	

suppresses the precipitation of the low-temperature (Nb_3Al) phase during cooling in the two-phase region and retains the high-temperature (Nb_{ss}) phase. Upon reaching a critical temperature, the Nb_{ss} transforms into Nb_3Al with the same composition without the need for long-range diffusion.

Present observations on the phase transformation sequence in the Nb–18 at.% Al alloy, namely: (i) heterogeneous nucleation of Nb_3Al at grain boundaries; (ii) time-dependent growth of the lamellar structure and (iii) compositional differences between Nb_{ss} and Nb_3Al precipitates, however, suggest that the process is diffusion controlled, which supports a nucleation and growth mechanism. This implies that either: (a) the 1800°C heat treatment did not form a complete solution and the existing Nb_{ss} is below the composition that could be cooled into the Nb_3Al region; (b) the 15°C/min cooling rate is sufficiently slow to allow for oriented nucleation and growth, or (c) aluminum loss during high-temperature processing results in an alloy composition below which Nb_3Al transforms massively. EDS measurements of the overall alloy composition tend to support the latter explanation.

3.3 Crystallography and growth orientation

Selected-area-diffraction patterns for the Nb_{ss} matrix and the Nb_3Al precipitates in the 24 h aged condition, are shown in Fig. 3. Analysis of the patterns reveal that the orientation relationship is described by $<110>_{Nbss}//<211>_{Nb_3Al}$; in other words, the Nb_3Al precipitate and Nb_{ss} matrix phases grow along the $<211>$ and $<110>$ directions, respectively. Other studies have reported $<110>_{Nbss}//<110>_{Nb_3Al}$ to be the favored orientation relationship.[20] The $<110>_{matrix}$ directions are preferred because dislocations lie on the {110} planes in bcc structures; incoherency strains across the interface can be relieved to decrease interfacial energy by aligning and generating dislocations.

The $<211>$ precipitate direction is believed to be the preferred growth direction for two reasons: Firstly, as shown in Table 1, the {211} planar spacings for Nb_3Al fit with {110} spacings of the Nb_{ss} matrix with only a 7% mismatch. The misfit strain parallel to the interface can be accommodated by a series of edge dislocations along the {110} planes in the matrix (Fig. 4). Secondly, $<211>$ directions in the precipitate are preferred over $<210>$ (which show a slightly better fit, see Table 1), because the {211} planes have a three-fold symmetry with 60°

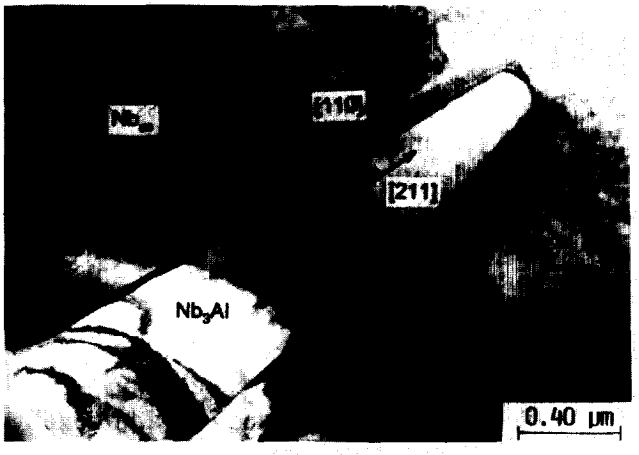

Fig. 4. High-magnification TEM micrograph of an Nb_3Al precipitate growing in the Nb_{ss} matrix. Note the array of edge dislocations along the interface between Nb_{ss} and Nb_3Al.

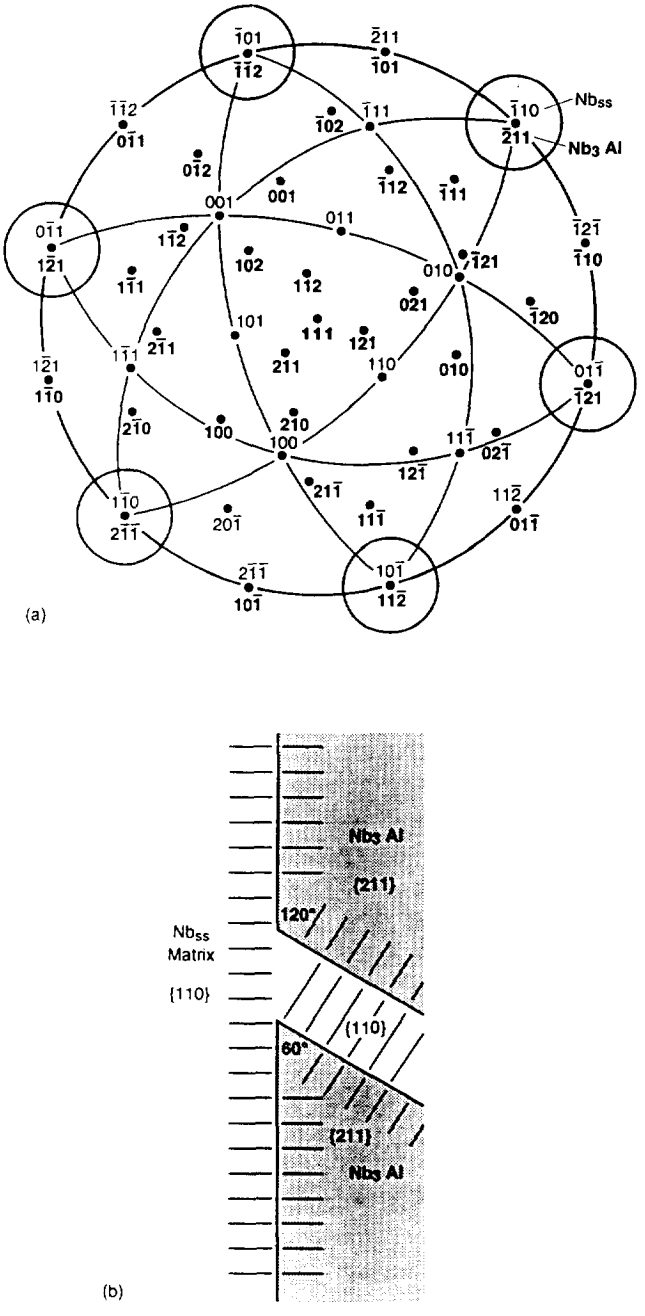

Fig. 5. (a) Stereographic projection with Nb_3Al (111) zone axis superimposed over a Nb_{ss} (111) zone axis such that (111) $(110)_{Nb}//(211)_{Nb_3Al}$, (see Figs 6 (a, b)). Note that the similar three-fold symmetry results in several sets of $\{110\}_{Nb}//\{211\}_{Nb_3Al}$. (b) Schematic illustration of how the similar three-fold rotational symmetry of {110} and {211} planes can allow for low energy interfaces to exist on multiple sets of $\{110\}_{Nb}$ and $\{211\}_{Nb_3Al}$ planes resulting in boundary angles of either 60 or 120°.

angles between planes, similar to {110} planes in the matrix. With this orientation compatibility, it is possible to form low energy semi-coherent interfaces on multiple sets of $\{110\}_{matrix}$ and $\{211\}_{Nb_3Al}$ planes, as illustrated in Fig. 5. As a result, boundaries between Nb_3Al and Nb_{ss} are expected at angles of 60 or 120°, as shown in Fig. 3, where Nb_3Al precipitates have multiple interfaces between the $\{110\}_{Nbss}$ and $\{211\}_{Nb_3Al}$. For the latter case, it is believed that two separate Nb_3Al grains grew together forming a perfectly coherent boundary between identically oriented planes of the {211} type, as shown schematically in Fig. 5(b).

Precise measurements between the <110> directions in the matrix and the <211> directions in Nb_3Al, determined from the selected-area diffraction patterns (Fig. 3), reveal a slight misorientation of ~7°, consistent with previously reported observations of 3–5° in this system.[20] Such distinct matrix/precipitate growth orientation relationship seen in the thermally treated, P/M processed Nb–Al alloy is also characteristic of a diffusion controlled nucleation and growth transformation.

Additional TEM observations include the abundance of dislocations in the Nb_{ss} matrix and bend contours in the Nb_3Al (Figs 3 and 4). The features result from the differing abilities of the two phases to react to volumetric dilational stresses associated with the transformation and thermal stresses generated upon cooling due to the mismatch in thermal-expansion coefficients. The ductile, bcc, Nb_{ss} matrix responds by generating dislocations to relieve these stresses. The brittle Nb_3Al intermetallic, however, has a complex A-15 crystal structure which restricts dislocation motion; instead, the Nb_3Al phase remains under residual strain which gives rise to bend contours.

3.4 Mechanical properties

The lamellar Nb/Nb_3Al composite microstructure of the Nb–18at.%Al alloy exhibits a Rockwell C hardness of ~55, (estimated yield strength of ~166 MPa), and a fracture toughness of K_{Ic} ~5·5 $MPa\sqrt{m}$. In contrast, unreinforced Nb_3Al has a K_{Ic} of 1·1 $MPa\sqrt{m}$ with an estimated yield strength of ~292 MPa.[12,13] The five-fold increase in toughness shown by the *in situ* Nb/Nb_3Al composite compared to pure Nb_3Al can be attributed primarily to the role of uncracked ductile Nb_{ss} ligaments in the crack wake (Fig. 6). Toughening of Nb_3Al arises from bridging tractions produced

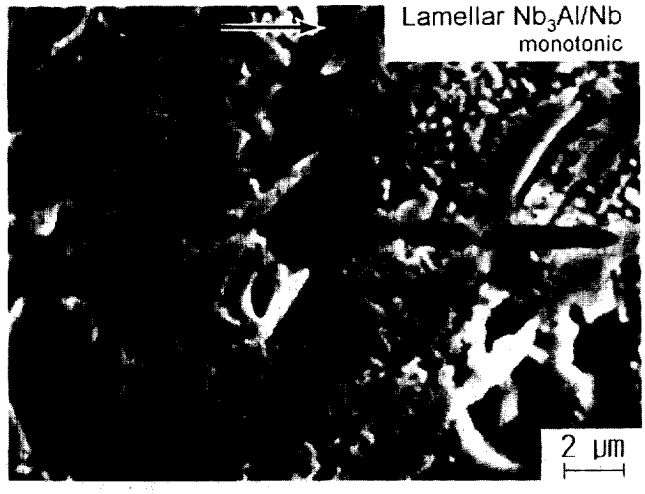

Fig. 6. SEM micrograph of the crack profile in the lamellar Nb/Nb_3Al composite microstructure under monotonic loading, showing crack bridging by the ductile Nb_{ss} phase in the crack wake. Arrow indicates the direction of crack growth.

by the uncracked ligaments and plastic deformation of the Nb_{ss} phase, thereby shielding the crack tip from remote loads; crack trapping and renucleation effects provide additional toughening.

The measured increase in toughness is consistent with simple crack-bridging models[7–10] that relate the increase in toughness to the area fraction of ductile phase ligaments intersecting the crack path (f), elastic modulus of the composite (E), yield strength (σ_y) and representative microstructural dimension (t) of the reinforcing phase. The increase, ΔK_c is given as:

$$\Delta K_c = \sqrt{Eft\sigma_y\chi} \qquad (1)$$

where χ is a dimensionless function representing the work of rupture (χ varies between 0·5 and 8, depending on interfacial bonding and properties of the reinforcement[7,10]). For the present lamellar Nb/Nb_3Al microstructure, taking f ~0·4, σ_y ~90 MPa, E ~123 GPa, Nb lamellar thickness t ~ 1 μm and χ ~2·7 (assuming a well bonded interface[9]), the predicted elevation in toughness from bridging is roughly 3·5 $MPa\sqrt{m}$. Using K_{Ic} for monolithic Nb_3Al as 1·1 $MPa\sqrt{m}$, the toughness of the Nb/Nb_3Al composite is ~4·6 $MPa\sqrt{m}$, which is slightly lower than the experimental value. Crack deflection, interfacial debonding and specifically crack trapping and renucleation across the ductile phase are expected to additionally contribute to toughness similar to observations made on equiaxed Nb/Nb_3Al composite microstructures.[13,14]

4 CONCLUSIONS

Based on a experimental study on the development of an *in situ* ductile-particle reinforced Nb/Nb_3Al intermetallic composite microstructure in a Nb–18at.%Al alloy, fabricated by powder processing and thermal treatment, the following conclusions can be made:

1. The evolution of the two-phase *in situ* Nb/Nb_3Al composite microstructure occurs through nucleation and growth controlled mechanisms involving long-range diffusion and not a massive transformation. This is corroborated by evidence of heterogeneous nucleation of Nb_3Al along niobium solid solution (Nb_{ss}) grain boundaries, slow kinetics of growth, compositional differences between Nb_{ss} matrix and Nb_3Al phases and observation of specific crystallographic orientation relationships between the matrix and precipitate phases.
2. The growth of Nb_3Al colonies from a supersaturated Nb_{ss} matrix progresses along the $<110>_{Nb_{ss}}$ matrix and $<211>_{Nb_3Al}$ precipitate directions. Such directions are preferred since they offer the least mismatch in interplanar spacing with identical three-fold symmetry.
3. Abundant dislocations in the Nb_{ss} matrix and extensive bend contours in the Nb_3Al intermetallic precipitates are evident from residual strains associated with the phase transformation and thermal mismatch stresses, respectively. Planar mismatch across the interface is accommodated by a series of edge dislocations.
4. The dual-phase, Nb/Nb_3Al lamellar composite microstructure displays a five-fold increase in toughness compared to pure Nb_3Al, primarily due to crack-bridging effects associated with the incoporation of the ductile Nb_{ss} phase.

ACKNOWLEDGEMENTS

This work was supported by the United States Air Force Office of Scientific Research under Grant No. F49620-93-0107 with Dr C. H. Ward as program manager. Our thanks to Drs C. H. Ward and A. H. Rosenstein of AFOSR for their continued support and Prof. L. C. DeJonghe at the University of California at Berkeley for helpful discussions.

REFERENCES

1. Stephens, J. J., *J. Metals*, **42**(8) (1990) 22.
2. Kattner, U. R., cited in *Alloy Phase Diagrams*, ASM Handbook, vol. 3, ASM International, Materials Park, OH, 1992, p. 2.48.
3. Anton, D. L., Shah, D. M., Duhl, D. N. & Giamei, A. F., *J. Metals*, **41**(9) (1989) 12.
4. Anton, D. L. & Shah, D. M., *High Temperature Ordered Intermetallic Alloys III*, eds C. T. Liu, A. I. Taub, N. S. Stoloff & C. C. Koch, Materials Research Society Conference Proceedings, Vol. 133, Materials Research Society, Pittsburgh, PA, 1989, p. 361.
5. Liu, C. T. & Stiegler, J. O., *Science*, **226** (1984) 636.
6. Schulson, E. M., *Int. J. Powder. Met.*, **23**(1) (1987) 25.
7. Ashby, M. F., Blunt, F. J. & Bannister, M., *Acta Metall.*, **37** (1989) 1847.
8. Mendiratta, M. G., Lewandowski, J. J. & Dimiduk, D. M., *Metall. Trans. A*, **22A** (1991) 1573.
9. Dève, H. E., Evans, A. G., Odette, G. R., Mehrabian, R., Emiliani, M. L. & Hecht, R. J., *Acta Metall.*, **38** (1990) 1491.
10. Elliott, C. K., Odette, G. R., Lucas, G. E. & Sheckherd, J. W., *High Temperature/High Performance Composites*, eds F. D. Lemkey, A. G. Evans, S. G. Fishman, and J. R. Strife, MRS Conference Proceedings, Vol. 120, Materials Research Society, Pittsburgh, PA, 1988, p. 95.
11. Flinn, B. Rühle, M. & Evans, A. G., *Acta Metall.*, **37** (1989) 3001.
12. Sigl, L. S. & Exner, H. E., *Metall. Trans. A*, **18A** (1987) 1299.
13. Murugesh, L., Venkateswara Rao, K. T. & Ritchie, R. O., *Materials Science and Engineering A*, 1994, in press.
14. Murugesh, L., Venkateswara Rao, K. T. & Ritchie, R. O., *Scripta Metall. Mater.*, **27** (1993) 1107.
15. Rowe, R. G. & Skelly, D. W., *Intermetallic Matrix Composites II*, eds D. Miracle, J. Graves and D. Anton, MRS Conference Proceedings, Vol. 273, Materials Research Society, Pittsburgh, PA, 1992, p.411.
16. ASTM Standard E399-90, *ASTM Standards*, Vol. 3.01, American Society for Testing and Materials, Philadelphia, PA, 1992, p. 506.
17. Hong, M., Ph.D. Thesis, University of California, Berkeley, 1980.
18. Lundin, C. E. & Yamamoto, A. S., *Trans Met. Soc. AIME*, 1966, Vol. 236, p.863.
19. Porter, D. A. & Easterling, K. E., *Phase Transformations in Metals and Alloys*, Van Nostrand Reinhold (International) Co. Ltd, Wokingham, Berkshire, UK, 1988, p. 349.
20. Marieb, T. N., Kaiser, A. D., Nutt, S. R., Anton, D. L. & Shah, D. M., *High Temperature Ordered Intermetallic Alloys IV*, eds L. A. Johnson, D. P. Pope & J. O. Stiegler, Materials Research Society Conference Proceedings, vol. 213, Materials Research Society, Pittsburg, PA, 1991, p. 329.